ELSEVIER

International Journal of Solids and Structures 41 (2004) 5125–5142

INTERNATIONAL JOURNAL OF SOLIDS and STRUCTURES

www.elsevier.com/locate/ijsolstr

Determination of elastic stresses from discrete data on stress orientations

A.N. Galybin [a,*], Sh.A. Mukhamediev [b]

[a] *School of Civil and Resource Engineering, M051, The University of Western Australia, 35 Stirling Highway, Crawley, WA 6009, USA*

[b] *Laboratory of Geomechanics, The Institute of Physics of the Earth, 10 Bol. Gruzinskaya str., Moscow 123810, Russia*

Received 23 October 2003; received in revised form 26 March 2004
Available online 6 May 2004

Abstract

The problem considered in this paper deals with reconstruction of stress fields in a plane elastic domain from discrete data on stress orientations. The problem is reduced to the determination of unknown coefficients in linear combinations of holomorphic functions used for the representation of complex potentials in plane elasticity. The coefficients are found by fitting the data to the calculated principal directions. This leads to an overdetermined system of linear algebraic equations which elements are subjected to experimental errors. The system is homogeneous; therefore, the coefficients cannot be determined uniquely. However, it allows for the unique reconstruction of stress trajectories. The determination of maximum shear stresses is non-unique: it can be multiplied by (i) an arbitrary real positive constant if principal directions are non-harmonic function of spatial coordinates; or (ii) a real valued positively defined bi-holomorphic function that depends on four real constants if principal directions are harmonic. The determination of the mean stresses is performed by integration, which introduces another real additive constant into the complete solution.

The proposed technique is capable of identification of singular (isotropic) points in the field of stress trajectories. This is illustrated in examples that use for the reconstruction either synthetic or real data from photoelasticity and geophysics.

Keywords: Elasticity; Principal directions; Stress trajectories; Stresses

1. Introduction

In geophysics, the discrete data on principal directions are used to compose stress trajectories (e.g., Hansen and Mount, 1990) or as the input for modelling tectonic stress fields in the earth's crust (e.g., Coblentz et al., 1995). Stress orientations can be specified by introducing so called (Timoshenko and Goodier, 1970) principal directions of a plane symmetric stress tensor as the angles of inclination of

* Corresponding author. Tel.: +1-618-9380-2631; fax: +1-618-9380-1044.
E-mail address: galybin@cyllene.uwa.edu.au (A.N. Galybin).

0020-7683/$ - see front matter © 2004 Elsevier Ltd. All rights reserved.
doi:10.1016/j.ijsolstr.2004.04.007

principal stress axes to any reference direction. Continuous fields of principal directions can directly be used for the determination of elastic stress fields, for instance, in photoelasticity this is achieved by integration of the equation of equilibrium (e.g., Frocht, 1941). This paper presents an alternative approach for the determination of elastic stresses in plane elasticity. It does not require integration and uses the principal directions at discrete points to uniquely determine trajectories of elastic stresses while other characteristics of the stress field are found with minimum arbitrariness.

The concept of stress trajectories comes from photoelasticity, therefore one can adopt the following definition due to Frocht (1941): stress trajectories or isostatics are curves the tangents to which represent the directions of one of the principal stresses at the points of tangency. Since there exist two mutually orthogonal principal directions at each point, stress trajectories can be viewed as curvilinear coordinate lines. This concept is widely used in photoelasticity for separation of principal stresses σ_1 and σ_2 from the Lame–Maxwell equations of equilibrium

$$\frac{\partial\sigma_1}{\partial s_1}+\frac{\sigma_1-\sigma_2}{\rho_2}=0, \qquad \frac{\partial\sigma_2}{\partial s_2}+\frac{\sigma_1-\sigma_2}{\rho_1}=0 \tag{1}$$

Here s_k are arc lengths along stress trajectories, $\rho_k=(\partial\theta_k/\partial s_k)^{-1}$ are radii of curvature of the stress trajectories, θ_k are principal directions, subscript $k=1,2$ is introduced in order to distinguish families of stress trajectories.

System (1) constitutes a complete system of partial differential equations for the determination of two principal stresses provided that the stress trajectories are known. This system is of hyperbolic type with the stress trajectories being the characteristics of it, thus either Cauchy or Goursat boundary value problems may be posed for the determination of principal stresses (e.g., Mukhamediev, 1991). It should be noted that in photoelasticity the maximum shear stress, $\tau_{\max}=|\sigma_1-\sigma_2|/2$, is also observed; therefore, in principle, any one of these equations can be used as, for instance, in the classical Filon's method. The problem of separation of principal stresses is discussed in detail in Frocht (1941), Coker and Filon (1957), Alexandrov and Akhmetzyanov (1973), Kuske and Robertson (1974) and other monographs on the photoelastic method. In any case, the magnitudes of boundary stresses have to be engaged in the separation of principal stresses by integration of system (1).

It is evident that no constitutive relationships are required for solving system (1). Therefore, solutions found from this system alone can be attributed to any material regardless of its mechanical behaviour. In photoelasticity, it is proposed (Alexandrov and Akhmetzyanov, 1973; Kuske and Robertson, 1974) to verify the results obtained after integration of (1) by satisfying some differential equations of the second order obtained by manipulations with the equations of equilibrium and the compatibility conditions. The latter in the case of the absence of body forces can be replaced by Laplace's equation

$$\Delta(\sigma_1+\sigma_2)=0 \tag{2}$$

Therefore in photoelasticity, the equation responsible for constitutive behaviour is used in order to check the accuracy of the results obtained when separating principal stresses rather than the third equation imposed on two unknown principal stresses.

The complete system of equations (1) and (2) represents an ill-posed problem provided that stress orientations are known within elastic regions. Galybin and Mukhamediev (1999) showed that given stress orientations and curvatures of stress trajectories on the boundary, one faces a non-classical boundary value problem of plane elasticity that can have a certain number of linearly independent solutions or be unsolvable. This depends upon the index, $2K$, of the problem that can be defined as the increment gained by any one of two principal directions after the complete counterclockwise traverse of the boundary of a simply connected domain. The increment is calculated in radians, divided by π, it is an integer or zero. In particular, it was found that for $2K<-1$ no solutions exist, for $2K=-1$ there exist a unique solution and four solutions exist for $2K=0$. This analysis supports the fact that the knowledge of stress trajectories

within the domain is redundant and leads to an ill-posed problem. It will be seen later that the application of proper methods for solving ill-posed problems is required; however, there is no need to formulate a boundary value problem in terms of stresses in order to solve the system (1) and (2).

Although this approach might be of less significance as far as photoelasticity is concerned (since it is already known that the model is elastic and (2) should be satisfied), it can be vital for other applications of the stress trajectory concept especially if stress orientations are known at discrete points rather than continuously. In geophysics, for example, the problem of determination of stress fields from known orientations of principal stresses is of great significance. Experimental data on in situ stresses are obtained by direct instrumental measurements such as overcoring or hydraulic fracturing as well as retrieved from the analysis of natural stress indicators as focal mechanisms of earthquakes, alignments of geological bodies, geometry and kinematics of fracture structures in the crust, stress induced borehole "breakouts", etc. Reliable data on the stresses in the earth's crust have been summarized and incorporated into the world stress database (Reinecker et al., 2003). These observations indicate that two of three principal stresses in the upper earth's crust are usually sub-horizontal (e.g., Zoback et al., 1989). Thus, 2D elastic problems are frequently employed in modelling of regional stress states (e.g., Coblentz et al., 1995).

In contrast to the photoelastic method that provides a continuous field of stress trajectories with certain accuracy, the orientations of stresses in the earth's crust are known at some discrete points with much worse accuracy due to various reasons. If data are dense enough, then a smooth continuous field of stress trajectories can be compiled by statistical and interpolation methods (e.g., Hansen and Mount, 1990; Lee and Angelier, 1994). However, it should also be noted that the presence of isolated singular points significantly complicates the problem. At such points (also known as isotropic points in photoelasticity, e.g., Frocht, 1941) stresses are hydrostatic, $\sigma_1 = \sigma_2$, thus, stress orientations are undetermined. Moreover, in a general case, the field of stress trajectories obtained by this manner cannot further be used in elastic modelling since Eq. (2) may not be satisfied, while it can be suitable for an inelastic material. This indicates that the known field of stress trajectories is, in some sense, a substitution for constitutive equations.

Therefore, the recovering of elastic stress trajectories should obey the complete system of elastic equations, for instance, in the form presented by (1) and (2). This is the main feature that differs the present study from other approaches based on pure mathematical methods alone regardless of governing equations for the considered material. Another important element is that the proposed procedure allows for the simultaneous determination of the maximum shear stress to be determined with minimum arbitrariness.

2. Formulation of the problem

Let Ω be a simply connected elastic domain bounded by a closed contour. This domain can be a subdomain of a bigger domain, which is not necessary simply connected and bounded. Let orientations of principal stresses (principal directions, θ_k) be known in a set of discrete points z_j ($j = 1, \ldots, N$) located within Ω. It is assumed that all these data are related to only major (minor) principal stresses; therefore, sub-index k in the notation for principal directions can be omitted further on. The general problem is formulated as follows: find an elastic stress field within Ω that provides minimum deviation of calculated principal directions from the data. This task requires minimisation of a certain functional as described in the next section.

No formal restrictions on distributions of data points over the domain are imposed: the distribution can be regular (e.g., data points at nodes of regular grid), uniform (e.g., random points uniformly distributed within the domain), irregular and non-uniform or data points can form clusters. Examples are presented in Fig. 1 and later on. In order to characterise the degree of data uniformity one can introduce a characteristic area $\Delta = S_\Omega/N$, where S_Ω is area of the domain. After that, the data density function can be obtained by calculating the number of data points over the moving square of the size $\Delta^{1/2}$. Large variations of this

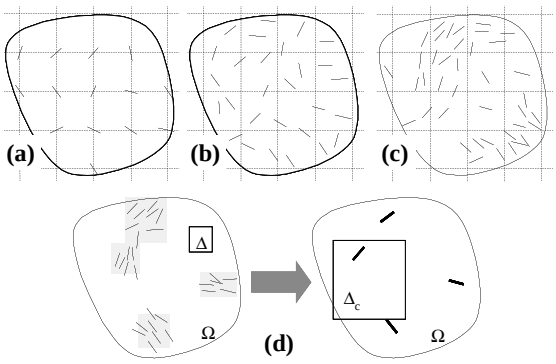

Fig. 1. Regular (a), uniform (b), irregular and non-uniform data (c), homogenisation of clustered data (d) (casters are shaded).

function indicate non-uniformity of the data distribution. Boundaries of clusters are associated with narrow zones of high gradients of the data density function.

The size $\Delta^{1/2}$ can also be associated with the characteristic length of redistribution of principal directions. As far as clusters are concerned, one can introduce another characteristic area, $\Delta_c = S_\Omega/N_c$, where $N_c > 0$ is the number of clusters identified, Fig. 1. It is evident that $\Delta_c > \Delta$, therefore the size $\Delta_c^{1/2}$ characterises the redistribution of principal directions at a larger scale. If each cluster is counted as a single datum, then the introduction of the second characteristic size $\Delta_c^{1/2}$ can be considered as a method of data homogenisation, i.e. clusters are absent at the larger scale as illustrated in Fig. 1d. In this case, solutions should be sought from a smoother class due to effective reduction in data, which provides averaging the principal directions within the clusters.

General solutions of plane elasticity can be expressed by means of two holomorphic functions $\Phi(z)$ and $\Psi(z)$ of complex variable $z \in \Omega$, and stress components are found via the Kolosov–Muskhelishvili formulae (Muskhelishvili, 1953)

$$\begin{aligned} &\frac{\sigma_{xx}+\sigma_{yy}}{2} = \Phi(z) + \overline{\Phi(z)} \\ &\frac{\sigma_{yy}-\sigma_{xx}}{2} + \mathrm{i}\sigma_{xy} = \bar{z}\Phi'(z) + \Psi(z) \end{aligned} \tag{3}$$

Hereafter the body forces are absent. This solution satisfies the equations of equilibrium and the elastic equation acknowledging the fact that the mean stress is a harmonic function inside the domain.

By introducing the following stress functions of complex variables $z = x + \mathrm{i}y$ and $\bar{z} = x - \mathrm{i}y$

$$\begin{aligned} &P(z,\bar{z}) = \Phi(z) + \overline{\Phi(z)} \\ &D(z,\bar{z}) = \bar{z}\Phi'(z) + \Psi(z) \end{aligned} \tag{4}$$

one can present the complete system of elastic equations as follows

$$\frac{\partial P(z,\bar{z})}{\partial z} = \frac{\partial D(z,\bar{z})}{\partial \bar{z}}, \qquad \frac{\partial^2 P(z,\bar{z})}{\partial z \partial \bar{z}} = 0 \tag{5}$$

Here the first equation is complex, it represents two scalar equations of equilibrium; the second one is Laplace's equation (2) written in variables z and $\bar{z}$; the differentiation with respect to complex variables is performed in accordance with the following rule

$$\frac{\partial}{\partial z} = \frac{1}{2}\left(\frac{\partial}{\partial x} - \mathrm{i}\frac{\partial}{\partial y}\right), \qquad \frac{\partial}{\partial \bar{z}} = \frac{1}{2}\left(\frac{\partial}{\partial x} + \mathrm{i}\frac{\partial}{\partial y}\right) \tag{6}$$

After differentiating the first equation in (5) with respect to conjugated variable it becomes evident that the elastic problem can be formulated in terms of the stress deviator function $D = D(z,\bar{z})$ alone as follows

$$\frac{\partial^2 D(z,\bar{z})}{\partial \bar{z}^2} = 0 \tag{7}$$

The harmonic function P does not affect principal directions; therefore, it is not included in the formulation of the problem. It can be found by integration of (5) and hence once the stress deviator is determined, the complete stress tensor becomes known. It should be noted however that the integration introduces an additive real constant, that is arbitrary and cannot be determined from the data on principal directions. It is also evident from that the equality of the imaginary part of the left-hand side of (7) to zero is simply a consequence of two scalar equations of equilibrium; it is valid for both elastic and non-elastic domains.

The stress deviator function $D = D(z,\bar{z})$ is represented in complex exponential form as follows

$$D(z,\bar{z}) = \tau(z,\bar{z})\,\mathrm{e}^{\mathrm{i}\alpha(z,\bar{z})} \tag{8}$$

where real valued functions $\tau = \tau(z,\bar{z})$ and $\alpha = \alpha(z,\bar{z})$ are modulus and argument of the stress function $D = D(z,\bar{z})$ respectively. The modulus is associated with the maximum shear stress $\tau_{\max}$; the argument is related to the principal directions, θ, as

$$\alpha(z,\bar{z}) = -2\theta(z,\bar{z}) \tag{9}$$

Principal directions of different families should not be mixed to insure that the modulus is non-negative; hereafter, θ is associated with the orientation of the minor principal stresses.

Once the argument α is found one can draw the field of stress trajectories by integrating the system of differential equations of the first order

$$\frac{\mathrm{d}z}{\mathrm{d}s_k} = \mathrm{e}^{\mathrm{i}\left(\theta(z,\bar{z})+(k-1)\frac{\pi}{2}\right)}, \quad k = 1,2 \tag{10}$$

Integration of (10) does not meet significant difficulties and can be performed numerically. Therefore the field of stress trajectories can be considered as known when the argument of D is known at any point of the domain, except singular points which will be analysed later in the subsection entitled singular points.

In the case of elasticity, the stress function D can be referred to as a bi-holomorphic function [1] in the view of the fact that it satisfies (7), i.e. its first derivative with respect to the conjugated variable is the holomorphic function $\Phi'(z)$ introduced above.

Now taking into account the expression of D via the holomorphic functions one can reduce the general mathematical formulation mentioned earlier to the problem of the determination of stress trajectories.

Given the argument of the stress deviator function D at discrete points z_j ($j = 1,\ldots,N$) as α_j, identify the function $\alpha = \alpha(z,\bar{z})$ that is close to α_j at the points z_j and represents itself as the argument of the bi-holomorphic function $D(z,\bar{z}) = \bar{z}\Phi'(z) + \Psi(z)$ everywhere inside the domain Ω including its boundary.

It is seen further that any solution of this elastic problem virtually determines the bi-holomorphic function D as well as the harmonic function P.

It should be noted that since not every function $\alpha = \alpha(z,\bar{z})$ satisfies elastic equations (Mukhamediev and Galybin, 2004), then one may expect certain difficulties solving the problem if α_j are chosen arbitrary, although an elastic solution can be found in this case as well due to the finite number of data.

[1] This definition is different from the definition of polyholomorphic (or polyanalytic) functions accepted in some mathematical works; for instance, Gakhov (1990) has introduced $\sum_{k=0}^{n}(z\bar{z})^k\varphi_k(z)$ as a polyanalytic function of nth order if φ_k are holomorphic. If such a definition has been used here then the holomorphic function $\Phi'(z)$ would have zero at the origin, which narrows the considered class of elastic problem.

3. Method of solution

3.1. Reduction to overdetermined system of linear algebraic equations

Solution is based on the following equality that takes place for the stress function D everywhere within the domain considered

$$\operatorname{Im}\left[\mathrm{e}^{-\mathrm{i}\alpha(z,\bar{z})}D(z,\bar{z})\right]=0,\quad z\in\Omega \tag{11}$$

Equality (11) is valid for both elastic and inelastic cases; it only expresses the fact that $\mathrm{e}^{-\mathrm{i}a}D$ is a real valued function, the modulus of D. In the case of elasticity considered here, one can take into account the second formula in (4) and rewrite (11) in terms of holomorphic functions as follows

$$\operatorname{Im}\left\{\mathrm{e}^{-\mathrm{i}\alpha(z,\bar{z})}\left[\bar{z}\Phi'(z)+\Psi(z)\right]\right\}=0,\quad z\in\Omega \tag{12}$$

Holomorphic functions $\Phi'(z)$ and $\Psi(z)$ are sough further in the form of linear combinations of linearly independent pre-assigned functions $R_k(z)$ that are also holomorphic in Ω.

$$\Psi(z)=\sum_{k=0}^{n}c_kR_k(z),\qquad \Phi'(z)=\sum_{k=0}^{n-1}c_{k+n+1}R_k(z) \tag{13}$$

Constants c_k are unknown and should be determined while solving the problem, after which the argument of the bi-holomorphic function becomes known as well as the function itself.

Note that in (13) the combinations for holomorphic functions may have different number of terms. It is assumed however that the representation for $\Phi'(z)$ has one term less than that for $\Psi(z)$, which is not compulsory but it will provide the same number of terms in both stress functions P and D. It also should be noted that $R_0(z)=1$ is used further, regardless of the choice of the other function $R_k(z)$.

Substitution of (13) into (4) leads to the following form for the bi-holomorphic function

$$D(z,\bar{z})=\bar{z}\Phi'(z)+\Psi(z)=\sum_{k=0}^{2n}c_kF_k(z,\bar{z}),\qquad F_k(z,\bar{z})=\begin{cases}R_k(z), & 0\leqslant k\leqslant n\\ \bar{z}R_{k-n-1}(z), & n<k\leqslant 2n\end{cases} \tag{14}$$

Eq. (14) being substituted into (12) results in the following functional equation

$$\operatorname{Im}\sum_{k=0}^{2n}c_k\,\mathrm{e}^{-\mathrm{i}\alpha(z,\bar{z})}F_k(z,\bar{z})=0,\quad z\in\Omega \tag{15}$$

Eq. (15) is further reduced to a system of linear algebraic equations with respect to unknown constants c_k. Since the function α is known at the points z_j one obtains by discretization of (15) the following system of N complex equations for the determination of $2n+1$ complex constants

$$\operatorname{Im}\sum_{k=0}^{2n}\mathrm{e}^{-\mathrm{i}\alpha_j}F_k(z_j,\bar{z}_j)c_k=0,\quad j=1,\ldots,N \tag{16}$$

Eq. (16) is a homogeneous one, thus at least one extra condition is required in order to find its non-trivial solution. As it is evident from formulae (11)–(16), the multiplication of (16) by any real constant does not violate this system, which means that any solution satisfying (16) can be normalised by a real constant. This constant can be chosen from the condition that the average modulus of D over the domain is unity. Since $|D|=\mathrm{e}^{-\mathrm{i}\alpha}D$, the extra equation assumes the form

$$\sum_{j=1}^{N}\sum_{k=0}^{2n} \mathrm{e}^{-\mathrm{i}\alpha_j} F_k(z_j,\bar{z}_j)c_k = N \tag{17}$$

It is convenient to rewrite system (16) and (17) in a matrix form by presenting the complex constants as $c_k = X_k + \mathrm{i}X_{2n+k+1}$ (and hence introducing a vector $\mathbf{X}$ of $4n+3$ real unknowns) and separating the real and imaginary parts of complex equations, which leads to

$$\mathbf{AX} = \mathbf{B} \tag{18}$$

where $\mathbf{A}$ is $(N+1)\times(4n+3)$ matrix of the system with the coefficients $A_{k,j}$ defined below; $\mathbf{X}$ is $(4n+3)$ vector of real unknowns X_k; and $\mathbf{B}$ is $(N+1)$ vector all components of which are zero except of the last one that is equal to N due to (17)

$$\begin{aligned} A_{j,k} &= \begin{cases} \mathrm{Im}\left[\mathrm{e}^{-\mathrm{i}\alpha_j} F_k(z_j,\bar{z}_j)\right], & 0 \leqslant k \leqslant 2n \\ \mathrm{Im}\left[\mathrm{i}\,\mathrm{e}^{-\mathrm{i}\alpha_j} F_{k-2n-1}(z_j,\bar{z}_j)\right], & 2n < k \leqslant 4n+1 \end{cases}, \quad j = 1,\ldots,N \\ A_{N+1,k} &= \begin{cases} \sum_{j=1}^{N} \mathrm{e}^{-\mathrm{i}\alpha_j} F_k(z_j,\bar{z}_j), & 0 \leqslant k \leqslant 2n \\ \sum_{j=1}^{N} \mathrm{i}\,\mathrm{e}^{-\mathrm{i}\alpha_j} F_{k-2n-1}(z_j,\bar{z}_j), & 2n < k \leqslant 4n+1 \end{cases} \end{aligned} \tag{19}$$

A redundant system (18) is solved further by the least squares method provided that $N \geqslant 4n+2$. However, this method alone is not able to ensure stability of the obtained solution caused, for instance, by the possible ill-posedness of the problem.

4. Solution of the linear system

It should be pointed out that the right-hand side of system (18), vector $\mathbf{B} = (0,\ldots,0,N)^{\mathrm{T}}$, is known exactly, while the coefficients of the matrix $\mathbf{A}$ depend on data quality. This situation is different from that specific for ill-posed problems of fitting, firstly because stability of solutions cannot be attributed to errors in the right-hand side and secondly because the matrix $\mathbf{A}$ is not necessary ill-conditioned. In the latter case, there is no need to apply any regularisation procedures common for ill-posed problems, as those presented in Tikhonov and Arsenin (1977). Therefore, it is proposed to control the condition number of matrix $\mathbf{A}$ during solving the system, which gives the indication whether the matrix is ill-conditioned or not.

There are two main sources that can make the matrix $\mathbf{A}$ to be ill-conditioned. First of all Eq. (17) does not guarantee that the rank of the system (18) is equal to $4n+3$ even if $N \geqslant 4n+2$. This special case is analysed in the next subsection. In addition, stress orientations expressed by the angles α_j are subjected to experimental errors that, in principle, can bring incorrectness into initially well-posed problem.

The method employed here eliminates both these sources automatically. It is based on the singular value decomposition method (see, e.g., Golub and Loan, 1989), which allows for easy control of the condition number, CN, defined as the ratio of largest and smallest singular values. If the condition number is greater than a specified critical value, CN^*, then the matrix $\mathbf{A}$ in (18) is replaced by a close matrix $\mathbf{A}'$ which rank is less that $\mathrm{rank}(\mathbf{A})$. The matrix $\mathbf{A}'$ is close to $\mathbf{A}$ in the sense that their greatest singular values coincide. This idea is widely used in image processing in order to reduce amount of data stored or transmitted (e.g., Andrews and Patterson, 1975; Forsythe et al., 1977; Kahar et al., 1989). Galybin (2002) has applied this approach for the regularisation of ill-posed problems of the identification of cohesive stresses in the process zone ahead of the crack tip and recovering of softening curves, in which matrix $\mathbf{A}$ was independent of input data. Specific details are presented below.

Firstly the singular value decomposition of $\mathbf{A}$ ($(N+1)\times(4n+3)$) is found in the form $\mathbf{A}=\mathbf{U}\mathbf{D}\mathbf{V}^{\mathrm{T}}$, where $\mathbf{U}$ ($(N+1)\times(N+1)$) and $\mathbf{V}$ ($(4n+3)\times(4n+3)$) are orthogonal matrices and $\mathbf{D}$ ($(N+1)\times(4n+3)$) is a diagonal matrix formed by the singular values, $d_j\geqslant 0$, placed in descending order, $d_1\geqslant d_2\geqslant\cdots\geqslant d_{4n+3}$. Secondly the matrix $\mathbf{D}$ is truncated by replacing least singular values by zeroes, which produces a diagonal matrix $\mathbf{D}'$ having rank K: $\mathbf{D}'=\mathrm{diag}\{d_1,d_2,\ldots,d_K,0\ldots0\}$ Then the matrix $\mathbf{A}'$ ($(N+1)\times(4n+3)$) of the rank K is determined as $\mathbf{A}'=\mathbf{U}\mathbf{D}'\mathbf{V}^{\mathrm{T}}$. Finally, the system in (18) is replaced by the system $\mathbf{A}'\mathbf{X}=\mathbf{B}$, solution of which is given by

$$\mathbf{X}=\mathbf{V}\mathbf{D}''\mathbf{U}^{\mathrm{T}}\mathbf{B} \tag{20}$$

Here $\mathbf{D}''$ is the diagonal matrix $(4n+3)\times(N+1)$ of the rank $K\leqslant n+3$: $\mathbf{D}''=\mathrm{diag}\{d_1^{-1},d_2^{-1},\ldots,d_K^{-1},0,\ldots,0\}$.

In the case $\mathrm{CN}\leqslant\mathrm{CN}^*$ no truncation of matrix $\mathbf{D}$ is performed, thus Eq. (20) provides exact solutions of initial system (18).

4.1. Harmonic argument

It follows from (4) and (8) that the argument α can be decomposed into the following sum

$$\alpha(z,\bar{z})=\arg\left(\Phi'(z)\right)+\arg\left(\bar{z}+\frac{\Psi(z)}{\Phi'(z)}\right) \tag{21}$$

The first term in the left-hand side of (21) is a harmonic function while the second term is the argument of a complex-valued harmonic function that, in general, it is not a holomorphic one. The total argument α is harmonic if the second term in (21) is omitted or constant. For instance, in the case of normally loaded half-plane or crack where $\Psi(z)=-z\Phi'(z)$, it is equal to $\pm\pi/2$. Circular boundaries present other examples that lead to the harmonic argument of the bi-holomorphic function. The general expression for this function can be taken in the form

$$D(z,\bar{z})=\left(a_0+a_1z+\bar{a}_1\bar{z}+a_2z\bar{z}\right)\chi(z),\qquad \mathrm{Im}(a_0)=\mathrm{Im}(a_2)=0 \tag{22}$$

where $\chi(z)$ is a holomorphic function. It should be noted the term in parenthesis in the right-hand side of Eq. (22) is a real valued function, thus the necessary condition is obvious; for the rigorous proof of sufficiency of the representation (22) see Mukhamediev and Galybin (2004).

Eq. (22) also shows that there are four real constants $(a_0,\mathrm{Re}(a_1),\mathrm{Im}(a_1),a_2)$ that do not affect stress trajectories in this special case. They cannot be determined by solving system (18), which manifests in the decrease of $\mathrm{rank}(\mathbf{A})$. For instance, if $\chi(z)=z$ and α_j are known exactly, $\mathrm{rank}(\mathbf{A})$ decreases by three units provided that the average modulus of D over the domain is unity, which eliminates one independent constant.

For continuous data, the direct substitution of $\alpha(z,\bar{z})$ into Laplace's equation verifies if argument is harmonic or not. With some tolerance, this can also be done for exactly known discrete data. However, the presence of experimental errors makes it impossible to distinguish a priori the case of harmonic and non-harmonic arguments. In applications, it can be recommended to seek solution from the class of non-harmonic arguments and check afterwards if the result indicates the harmonic argument. This can be achieved, for instance, by verifying a posteriori the following relationships between complex potentials that follow from (22)

$$(\bar{a}_1+a_2z)\Phi'(z)-(a_0+a_1z)\Psi(z)=0 \tag{23}$$

However, if there is no clear indication in data then, in principle, these two cases should be considered separately, followed by comparison of the results in order to decide between the two variants.

System (18) can be substantially simplified for the case (22). Thus, by substituting $\chi(z) = |\chi(z)|\,e^{i\arg[\chi(z)]}$ into (22), taking logarithm of both parts and separating the imaginary part one finds

$$\ln \chi(z) - \overline{\ln \chi(z)} = 2i\,\alpha(z,\bar{z}), \quad \alpha(z,\bar{z}) = \arg[\chi(z)] \tag{24}$$

Further, a linear system could be formed as described above, in which the only holomorphic function has to be determined. Moreover, the matrix of this system would be independent of α, thus the errors can only be attributed to the right-hand side of the system. This probably would be the best way to obtain a solution in the special case of harmonic argument, however it has been discarded because no singular points can be detected by this approximation as explained below.

4.2. Singular points

Singular points in stress trajectories can be separated into two classes. The first class is referred to the usually adopted meaning for singular points where stresses are discontinuous. The second class is referred to in photoelasticity as isotropic points at which principal stresses are equal to each other hence no principal directions exist. It should be noted that trajectories themselves can represent a continuous set of isotropic points, but in this case the boundary coincides with a trajectory as, for instance, in the case of a non-loaded isotropic plane having a crack which surfaces are subjected by normal loading. Hence, such cases do not present any difficulties in identification of singular points. Positions of singular points of the first class are also obvious for the case of notches, concentrated forces acting on the boundary or points of discontinuity in boundary conditions (concentrated forces and/or couples that act within the domain are exceptional). Therefore, the only isolated singular points of the second class (isotropic points) have to be identified in the field of stress trajectories being reconstructed from the discrete data.

Two types of isotropic points of the first order are usually observed in photoelasticity, although the existence of isotropic points of higher order is theoretically possible (e.g., Kuske and Robertson, 1974). These points can be classified in accordance with the asymptotic behaviour of the stress deviator function (Karakin and Mukhamediev, 1994) in the vicinity of its zero. Assuming this zero at the origin one has the following expansion

$$D(z,\bar{z}) = A\bar{z} + Bz + \cdots \tag{25}$$

If $|A| > |B|$ one has singular point of A-type and if $|A| < |B|$ then it is of B-type. Both these types may appear simultaneously within the considered domain as shown in Fig. 2 which represents a fragment of the

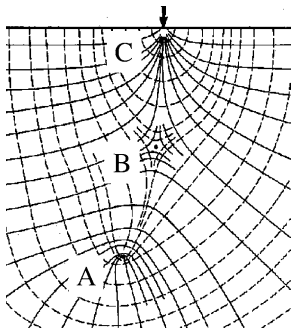

Fig. 2. Singular points in the field of stress trajectories: A—interlocking isotropic point (A-type), B—non-interlocking isotropic point (B-type), C—singular point under concentrated load. Fragment of trajectory field obtained in the experiment of bending of photoelastic beam, after Frocht (1941).

trajectory field obtained in a photoelastic beam under four point bending load (after Frocht, 1941). Note also the singular point C of the first class that corresponds to concentrated load on the boundary.

The following property of singular points should be pointed out. Let γ_A and γ_B be closed contours encompassing isotropic points of the A and B-type respectively and let no other singular points within these contours be present Then it is evident that principal directions gain an increment of $\pm\pi$ after the complete traverse of these contours respectively. Therefore the angle α, argument of D, gains the increment $-2(\pm\pi)$.

This property prohibits the application of Eq. (24) for the domains with isotropic points even if the argument is a harmonic function. This is due to the fact that the principle of argument for holomorphic functions (e.g., Gakhov, 1990) requires the compensation of the increment in the argument by introducing poles or zeroes within the contour. However, they are not present there. In principle, in the vicinity of an isotropic point, z_0, one might extract the factors $(z - z_0)$ or $(\bar{z} - \bar{z}_0)$ from the function $D(z, \bar{z})$ with the aim to make the rest holomorphic. However, this would require a priory identification of the isotropic points that is a separate problem. The approach based on (13) and (14) is free from these shortcomings and it allows for simultaneous recovering the isotropic point of the both types.

5. Model examples

5.1. Synthetic example: recovering of trajectories with singular points

This subsection presents an artificial example in which principal directions are modelled by a certain stress function $D_{\text{ideal}}(z, \bar{z})$ that is analytically defined in square domain $\Omega_s = \{|x| \leqslant 1, |y| \leqslant 1\}$. The stress function is calculated at a number of points to produce discrete data followed by the introduction of errors at each data point in order to model experimental observations. The scope of this section is to investigate the accuracy in the reconstruction of stress trajectories and stress functions as well as the possibility of recovering the isotropic points of both types mentioned above. For this purpose, the bi-holomorphic function D has been taken in the following simple form

$$D_{\text{ideal}}(z, \bar{z}) = C_0(z - C_1)\left(\bar{z} - \overline{C}_2\right) \tag{26}$$

where C_1 and C_2 are located within Ω_s. From the comparison of (26) and (25) it is evident that these points are isotropic points of B and A-types correspondingly.

Particular form for the ideal mean stress is taken in the form

$$P_{\text{ideal}}(z, \bar{z}) = \text{Re}[C_0 z(z - 2C_1)] \tag{27}$$

The discrete data are found from (26) as follows

$$\theta_j = -\tfrac{1}{2}\arg\left[D_{\text{ideal}}\left(Z_j, \overline{Z}_j\right)\right] + \eta_j \tag{28}$$

Data points Z_j $(j = 1, \ldots, N)$ have been introduced either regularly or randomly, but in the latter case they also have been uniformly distributed within the square Ω_s and generated by MathCAD 6 PLUS built-in procedure $\text{rnd}(x)$. The errors η_j have been generated by the procedure $\text{rnorn}(N, \text{mean}, \text{stdev})$ as random numbers normally distributed with zero mean and given standard deviation. The number of data points varies depending on the number of unknown coefficients in expansion (13) remaining $N = 10n$ in all calculations performed. Complex potentials $\Phi'(z)$ and $\Psi(z)$ in (13) have been sought as polynomials of n and $n - 1$ degrees respectively, i.e. $R_k(z) = z^k$ $(k = 0, \ldots, n)$.

The following characteristics have been used for the comparison of ideal and recovered stress functions:

- Dislocations of recovered singular points from ideal positions $\rho_k = |C_k - z_k^*|$, $k = 1, 2$, where z_k^* are two different roots of the equation $D_{\text{rev}}(z, \bar{z}) = 0$ found within the square Ω_s; they are numbered with respect to the closest singular point C_k.
- Deviation of ideal and recovered stress functions calculated as standard deviations of three arrays $\mathbf{\Delta M}$, $\mathbf{\Delta A}$ and $\mathbf{\Delta P}$ which elements represent the differences of ideal and recovered moduli ΔM and arguments ΔA of the stress deviator and mean stresses ΔP respectively at a set of points z_m ($m = 1 \ldots N_d$) regularly distributed within the square Ω_s, i.e. $\Delta M_m = |D_{\text{ideal}}(z_m, \bar{z}_m)| - |D_{\text{rec}}(z_m, \bar{z}_m)|$, $\Delta A_m = \arg(D_{\text{ideal}}(z_m, \bar{z}_m)) - \arg(D_{\text{rec}}(z_m, \bar{z}_m))$ and $\Delta P_m = |P_{\text{ideal}}(z_m, \bar{z}_m)| - |P_{\text{rec}}(z_m, \bar{z}_m)|$; note that the nodes Z_j and the points z_m are different.

In order to illustrate the results of reconstructions of the stress field an example is presented below in which the following parameters have been used $C_1 = 0.5 + 0.5\text{i}$, $C_2 = -0.5 - 0.3\text{i}$, $n = 4$, $N = 40$, $N_d = 100$. The errors introduced in this example were within the range $(-5.8°, 12.2°)$ with the standard deviation of stdev $= 5°$. Fig. 3 presents a pattern of one family of recovered stress trajectories, i.e. the angle $\theta = -0.5 \arg(D_{\text{rec}}(z, \bar{z}))$, and positions of singular points that are shown by symbols. The recovered trajectories are very close to the ideal ones; they are not shown in the figure, stdev$(\mathbf{\Delta A}) = 23.3°$ in this example. The following dislocations of the recovered singular points from the ideal ones have been found: $\rho_1 = 0.071$, $\rho_2 = 0.04$. Figs. 4 and 5 represent contour maps of ideal and recovered maximum shear stresses $\tau(z, \bar{z})$ and mean stresses, $P(z, \bar{z})$. The latter is obtained from $D_{\text{rec}}(z, \bar{z})$ by integrating the equations of equilibrium and omitting the additive constant (for the sake of comparison with (27), where this constant is not present). Both figures illustrate good agreement of ideal and recovered characteristics of the stress fields; in this example, stdev$(\mathbf{\Delta M}) = 0.138$, stdev$(\mathbf{\Delta P}) = 0.15$ and means of these arrays are zero, which is provided by the proper choice of the real multiplicative constant in the recovered solution, $D_{\text{rec}}(z, \bar{z})$.

Two other types of approximating functions R_k have also been examined: polynomials with random roots, $R_k(z) = \prod_{j=0}^{k} (z - c_j)^j$, $(c_j \in \Omega_s)$, and Legendre polynomials, $R_k(z) = P_k(z)$, $P_k(z) = \frac{1}{2^n n!} \frac{d^n}{dx^n} (x^2 - 1)^n$ that have roots on the real axis. No essential difference in results has been noticed.

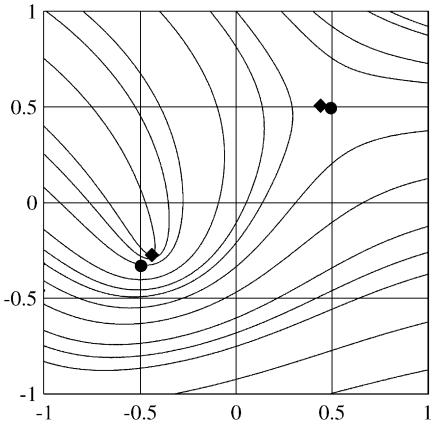

Fig. 3. Stress trajectories recovered from (28); circles are ideal positions of singular points, squares are recovered positions of singular points.

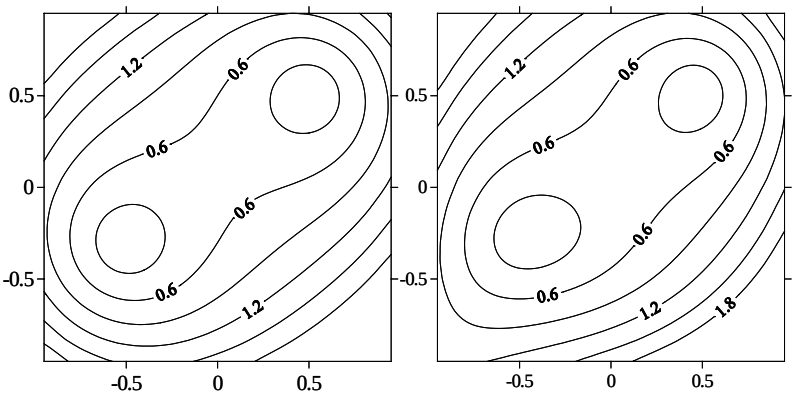

Fig. 4. Contour maps of ideal (left) and recovered (right) maximum shear stresses.

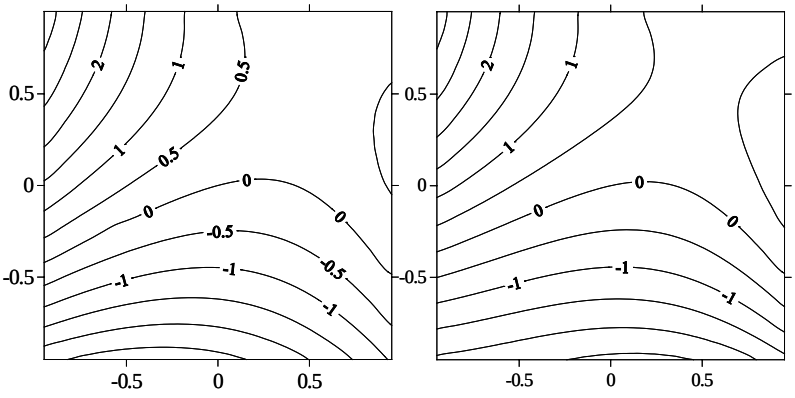

Fig. 5. Contour maps of ideal (left) and recovered (right) mean stresses.

5.2. Elastic disk: harmonic argument

This synthetic example illustrates the approach to the reconstruction of stress functions for the case of harmonic argument. The solution is sought in the class of harmonic arguments only regardless of errors introduced.

Let an elastic disk of unit radius be loaded along a diameter by two equal and opposite concentrated forces, p, then the bi-holomorphic function can be obtained from complex potentials presented by Muskhelishvili (1953) as follows

$$D_{\text{ideal}}(z,\bar{z}) = \frac{2p}{\pi}\frac{1-z\bar{z}}{(1-z^2)^2} \tag{29}$$

Here the real axis coincides with the direction of the applied forces.

It is evident from (29) that the argument of D_{ideal} is a harmonic function since the denominator of the fraction in (29) is holomorphic while its numerator is real valued. Therefore, any particular solution, $D_{\text{rec}}(z,\bar{z})$, reconstructed from the exactly known discrete data is not capable to recover the numerator of the

fraction in (29), which eventually leads to the general solution in the form (22) that contains up to four real constants.

The domain, Ω_h, analysed further is the square inscribed into the unite circle, i.e. $\Omega_h = \{z : |\mathrm{Re}(z)| < 2^{-1/2}, |\mathrm{Im}(z)| < 2^{-1/2}\}$. Contour map of maximum shear stresses and stress trajectories obtained from (29) within Ω_h are presented in Fig. 6 for $p = 1$. Further, they referred to as ideal modulus and ideal stress trajectories correspondingly The discrete data are found from (29) by formula (28) in which the nodes Z_j $(j = 1, \ldots, N)$ have been introduced regularly within the square, $Z_j \in \Omega_h$; in examples below $N = 100$. Noise, η_j, is modelled as in the previous subsection.

Despite the absence of singular points in the trajectory field (Fig. 6), no special programme has been developed for this case: solution is still sought in the form (14) by putting $F_k(z, \bar{z}) = 0$ for all $k > n$. This leads to the reduction of the dimension of the linear system to $(N + 1) \times (2n + 3)$ linear algebraic equations, which is achieved by setting the critical condition number $\mathrm{CN}^* = 10^5$ as described above. As the consequence of this, one still has the same restriction on the number of approximating functions, $4n + 2 \leqslant N$, i.e. $n \leqslant 24$ in this case.

Similarly to the previous subsection, three types of R_k have been examined: polynomials, polynomials with random roots and Legendre polynomials. No essential difference in results obtained with the use of different $R_k(z)$ has been noticed while $n \leqslant 16$ regardless of whether the noise is present or not. However, the analysis has shown that the condition number, CN, increases with the increasing number of approximation functions (parameter n). It has been found that for polynomials the increase is less than for the other two types used, for instance, for $n = 12$: $\mathrm{CN} = 6 \times 10^5$ for Legendre polynomials, CN varies in the range $(0.1–33) \times 10^3$ for different polynomials with random roots, while for polynomials $\mathrm{CN} = 51$. Therefore, $R_k(z) = z^k$ are used in this example, which provides better stability in recovering the stress function D_{rec}.

The result of fitting is obtained as a polynomial function $\chi_{\mathrm{rec}}(z)$ that is holomorphic in finite domain Ω_h. The arguments of $\chi_{\mathrm{rec}}(z)$ and $D_{\mathrm{ideal}}(z, \bar{z})$ in (29) are close to each other due to fitting, while their moduli are different because they are moduli of holomorphic and bi-holomorphic functions respectively. As it has been mentioned above, the general solution depends on four arbitrary real constants that cannot be determined from the data alone. The approximate solution that corresponds to the ideal one can be considered as a particular solution by specifying the coefficients a_0, $\mathrm{Re}(a_1)$, $\mathrm{Im}(a_1)$, a_2 in (22). For the case when $a_1 = 0$ and $a_2 = 0$ one obtains a solution by means of holomorphic function $a_0\chi_{\mathrm{rec}}(z)$. The modulus of this function is presented in Fig. 7a that is different from the ideal one shown in Fig. 6 (no noise was introduced). When coefficients are chosen as $a_1 = 0$, $a_0 = a_2 = a$, in order to address the fact that the discrete data were formed from a bi-holomorphic function (29), then solution assumes the form

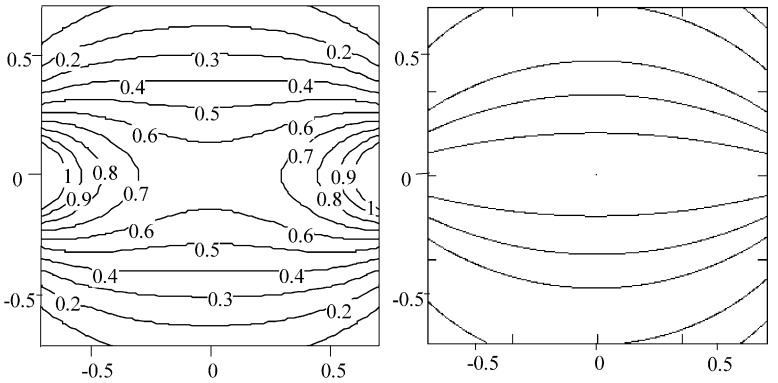

Fig. 6. Ideal contour map of modulus (left) and ideal trajectories (right) within the square Ω_h.

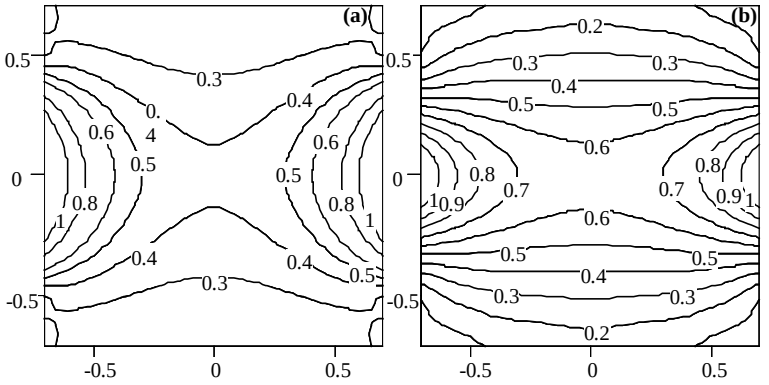

Fig. 7. Moduli, $n = 12$: without correction (left) with correction (right).

$$D_{\mathrm{rec}}(z,\bar{z}) = a(1 - z\bar{z})\chi_{\mathrm{rec}}(z), \quad \chi_{\mathrm{rec}}(z) = \sum_{k=0}^{n} c_k z^k \tag{30}$$

Contour map of $|D_{\mathrm{rec}}(z,\bar{z})|$ is shown in Fig. 7b for the case when no noise was added to the discrete data. The coefficient a is chosen such that $\mathrm{mean}(D_{\mathrm{ideal}}) = \mathrm{mean}(D_{\mathrm{rec}})$ in Ω_{h}, which provides better visual assessment of ideal and recovered contour maps of maximum principal stresses.

The analysis of different sets of noises that disturbs the data has been performed. It shows that the increase in the degree of polynomials from $n = 2$ to 12 leads to the better agreement between recovered and ideal characteristics, i.e. stress trajectories, maximum shear stresses and mean stresses. Further increase does not lead to the improvement of the results, which is explained by the loss of redundancy.

5.3. An example from photoelasticity

The field of trajectories depicted in Fig. 2 has been used to prepare discrete data for the reconstruction of stress trajectories and maximum shear stresses. For this purpose, the coordinates of intersection points of two families of mutually orthogonal trajectories have been digitised by software *Surfer* directly from the screen. After that, the principal directions have been obtained as the orientations of spans connecting the intersection points lying on the trajectories presented by solid lines. Therefore, two sources of errors have been introduced: by digitising procedure and by approximation of tangents by spans.

The domain considered represents itself the rectangle $|x| < 1$, $|y| < 1.057$. The input data is presented in Fig. 8a where principal directions are shown by 73 segments. The data is non-uniform and the presence of isotropic points is not evident from the figure.

Fig. 8b presents the reconstructed stress trajectories and singular points by the procedure described above in the previous sections for $n = 4$. The functions $R_k(z)$ used were as follows

$$R_k(z) = (z - z_{\mathrm{pole}})^{-2} z^k, \quad z_{\mathrm{pole}} = 0.2 + 1.4\mathrm{i} \tag{31}$$

The weight function in (31) has been chosen in order to address the existence of singular point C where the concentrated force is applied to the boundary, see Fig. 2. Although the point of application of this force is known exactly, here the position of this point has been chosen approximately in order to test whether this affects the results of the reconstruction.

Comparison of Figs. 8b and 2 demonstrate satisfactory agreement of both the singular points and stress trajectories obtained by photoelastic methods and recovered by the proposed procedure. It has been found that the example presented is not very sensitive to the accurate account for the position of singular points of C-

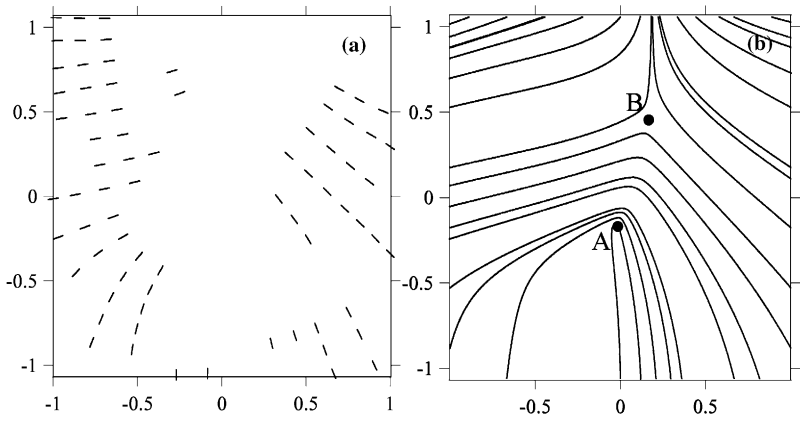

Fig. 8. Recovering of elastic stress trajectories and isotropic points for $n = 4$: (a) input data 73 points, no singular points specified, (b) recovered trajectories and singular points A and B.

type. However, the introduction of the weight function in (31) is beneficial and allows one to reconstruct stress trajectories more accurately than in the case without the weight function. It should be noted that the increase of the number of approximating functions used in reconstruction without the weight improves results, thus for $n = 10$ stress trajectories are somewhat similar to those presented in Fig. 8b. However, further increase of n leads to the substantial loss of redundancy, which affects the results and does not lead to improvement.

Maximum shear stresses are presented in Fig. 9. Fig. 9a shows a fragment of the stress pattern observed in photoelasticity. This fragment has been extracted from a complete pattern presented in Frocht (1941); it corresponds to the area for which the reconstruction of stress trajectories has been performed, i.e. to the region shown in Fig. 2. Fig. 9b illustrates the results of reconstruction of the modulus of the stress function D. Contour lines presented in this figure have been drawn with the intervals of 0.15 chosen to make the black areas in the middles of both figures be of similar sizes.

5.4. Geophysical application: Australian stress field

This subsection presents preliminary results of the investigation of the Australian stress field. Currently the database of stress orientations (Reinecker et al., 2003) has more than 13,600 data points around the

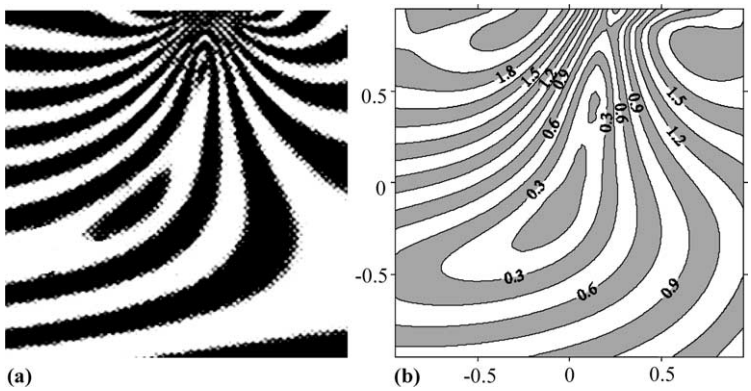

Fig. 9. Maximum shear stresses: (a) fragment of a stress pattern (extracted from Frocht, 1941); (b) contour map of recovered modulus of the stress function D.

globe at which orientations of principal stresses have been measured by a number of special methods. The data is of different quality ranging from E (low) to A (high). In this paper we use the data located within the region (−40° S, −10° S) and (110° W, 155° W) with the quality A, B and C (269 points in total). It should be noted that the data are non-uniform within the continent, which present an obstacle for the analysis. There are few clusters where the data are dense; they are shown in Fig. 10 by black rectangles. These clusters have been obtained by plotting a density function that was found by calculating the number of data points over the moving window of approximately $2°\times 2°$ in size with the step of 0.65°. This window size is chosen as the square root of the ratio of the area of the region and the number of data points; the step is three times less then the window size. It has been assumed that data form a cluster if five or more points are located within the window. This analysis indicates that the number of functions $R_k(z)$ in approximation (13) should not be very large. Consequently, if each cluster in Fig. 10 was considered as a single datum then it follows from $N > 4n + 3$ that $n = 2$ would have been used in the analysis. Coblentz et al. (1995) employed this way to reduce the data in their elastic finite-element modelling of Australian stress field, which also required the averaging of stress orientations over the marked areas. This procedure, however, strongly depends on the method applied; therefore in contrast to Coblentz et al. (1995) no averaging of data within the clusters has been performed.

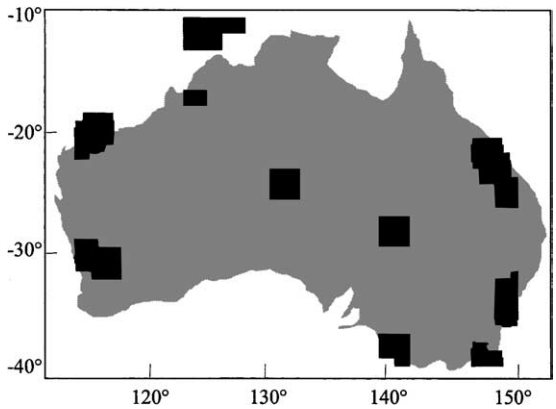

Fig. 10. Data clusters (five or more measurements available) within the investigated region.

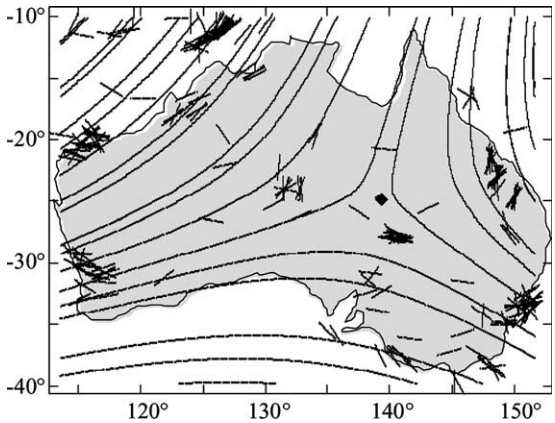

Fig. 11. Recovered trajectories and singular point (symbol) in Australia, $N_{\text{data}} = 269$, $n = 2$, data is presented by black segments.

In the present analysis polynomials were used as approximating functions, $R_k(z) = z^k$, their degrees were varied from $n = 1$ to 10. Fig. 11 illustrates the trajectory field obtained for the Australian continent in the case when $n = 2$.

In all cases considered, the presence of a singular point of the B-type within the continent has been revealed; it is shown in Fig. 11 by a small black rhombus. Position of this point slightly varies within the region (−28° S, −25° S) and (135° W, 139° W) for $1 < n \leqslant 10$ (−31° S, 144° W for $n = 1$). It should be noted that for $n > 4$ other singular points appears near the boundaries of the considered domain, however they are not stable, which indicates that these are not real but likely caused by inconsistence of clustered data and degree of polynomials.

5.5. Closure

Examples presented in the previous section demonstrate that elastic stress fields can be recovered with satisfactory accuracy from the discrete data on principal directions. It is proposed to fit the data to the calculated principal directions obtained from the general solution well known in plane elasticity. This approach allows one to undertake a revision of the methods used in photoelasticity in the problem of the separation of principal stresses from the stress trajectories. The separation can be performed without the integration of the equilibrium equations as currently used. The application of the proposed technique to the geophysical problem of the reconstruction of tectonic stresses in the earth's crust creates new perspectives in the analysis of geophysical data currently available.

Acknowledgements

The authors would like to acknowledge the support of the MNRF project "Australian Computational Earth System Simulator".

References

Alexandrov, A.Ya., Akhmetzyanov, M.H., 1973. Polarization and Optical Methods in Mechanics of Deformable Solids. Nauka, Moscow (in Russian).

Andrews, H.C., Patterson, C.L., 1975. Outer product expansions and their uses in digital image processing. Am. Math. Monthly 82, 1–13.

Coblentz, D.D., Sandiford, M., Richardson, R.M., Zhou, S., Hillis, R., 1995. The origins of the intraplate stress field in continental Australia. Earth Planet. Sci. Lett. 133, 299–309.

Coker, E.G., Filon, L.N.G., 1957. A Treatise on Photo-Elasticity. University Press, Cambridge.

Forsythe, G.E., Malcolm, M.A., Moler, C.B., 1977. Computer Methods for Mathematical Computations. Prentice Hall, Englewood Cliffs, New Jersey.

Frocht, M.M., 1941. In: Photoelasticity, vol. 1. John Wiley & Sons Inc., New York.

Gakhov, F.D., 1990. Boundary Value Problems. Dover Publication, New York.

Galybin, A.N., 2002. Determination of softening law by measuring crack opening displacements. In: Dyskin, A.V. et al. (Eds.), Structural Integrity and Fracture. Swets & Zeitlinger BV, Lisse, The Netherlands, pp. 35–41.

Galybin, A.N., Mukhamediev, Sh.A., 1999. Plane elastic boundary value problem posed on orientation of principal stresses. J. Mech. Phys. Solids 47, 2381–2409.

Golub, G.H., van Loan, C.F., 1989. Matrix Computations, second ed. The Johns Hopkins University Press, Baltimore/London.

Hansen, K.M., Mount, V.S., 1990. Smoothing and extrapolation of crustal stress orientation measurements. J. Geophys. Res. 95 (B), 1155–1165.

Kahar, D., Moler, C., Nash, S., 1989. Numerical Methods and Software. Prentice Hall, Englewood Cliffs, New Jersey.

Karakin, A.V., Mukhamediev, Sh.A., 1994. Singularities in nonuniform field of trajectories of the principal tectonic stresses. Izvestiya, Phys. Solid Earth 29, 956–965.

Kuske, A., Robertson, G., 1974. Photoelastic Stress Analysis. John Wiley & Sons, London.
Lee, J.-C., Angelier, J., 1994. Paleostress trajectory maps based on the results of local determinations: the "Lissage" program. Comput. Geosci. 20, 161–191.
Mukhamediev, Sh.A., 1991. Retrieving field of stress tensor in crustal blocks. Izvestiya, Phys. Solid Earth 27, 370–377.
Mukhamediev, Sh.A., Galybin, A.N., 2004. On reconstruction of stress fields from stress trajectories. Trans. (Doklady) Russ. Acad. Sci. 396 (1).
Muskhelishvili, N.I., 1953. Some Basic Problems of the Mathematical Theory of Elasticity. P. Noordhoff Ltd., Groningen, Holland.
Reinecker, J., Heidbach, O., Mueller, B., 2003. The 2003 release of the World Stress Map. Available from <www.world-stress-map.org>.
Tikhonov, A.N., Arsenin, V.Y., 1977. Solution of Ill-Posed Problems. Wiley & Sons, New York.
Timoshenko, S.P., Goodier, J.N., 1970. Theory of Elasticity, third ed. McGraw-Hill, New York.
Zoback, M.L., Zoback, M.D., Adams, J., et al., 1989. Global patterns of tectonic stress. Nature 341, 291–298.